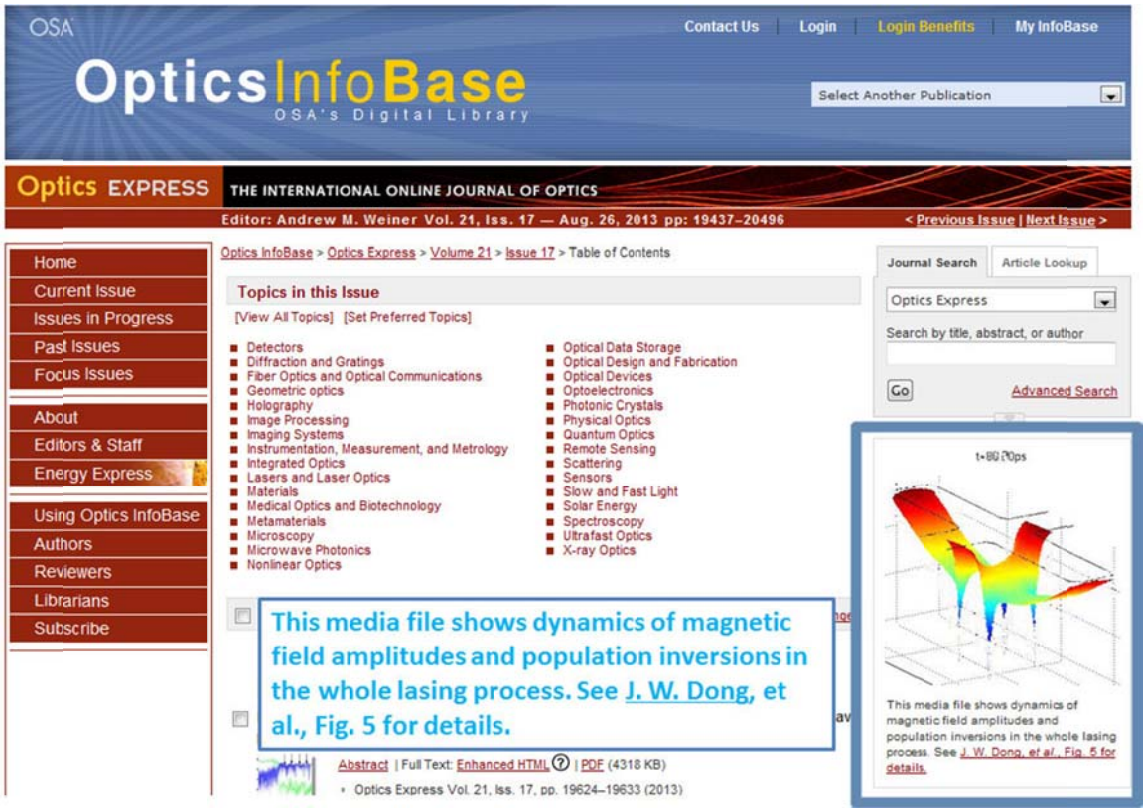

Lasing in plasmon-induced transparency nanocavity

Zi-Lan Deng and Jian-Wen Dong*

State Key Laboratory of Optoelectronic Materials and Technologies, Sun Yat-sen University, Guangzhou 510275, China

**dongjwen@mail.sysu.edu.cn*

Abstract: We propose a plasmon-induced transparency (PIT) nanocavity for achieving nanoscopic coherent light source. The compact cavity is constructed by a pair of detuned nano-stubs incorporated with four-level gain medium. The PIT response enables the reduction of the coupling loss from cavity to waveguide while keeping the cavity size unchanged, different from the end-facet Fabry-Pérot cavity in which the radiation loss decreases at the cost of size increment. In order to study the lasing behavior of surface plasmon wave in the PIT cavity, the self-consistent finite element method is employed to model the interactions between gain and propagating surface plasmons. The dynamics of the whole lasing process is observed, and the linear output-input relation is obtained for the single mode plasmon lasing. It is demonstrated that smaller stub-pair detuning provides stronger feedback inside the cavity. Consequently, the lasing threshold of pumping rate decreases quadratically with the decreasing of detuning. However, the output-input extraction efficiency will improve when the detuning is not so small. One of the advantages for the proposal is that the lasing output power from the cavity can directly couple towards the metal-dielectric-metal waveguide platform, facilitating the field of integrated plasmonic circuits and molecular-scale coherent light source.

#191661 - $15.00 USD Received 3 Jun 2013; revised 11 Aug 2013; accepted 16 Aug 2013; published 22 Aug 2013

Lasing in plasmon-induced transparency nanocavity

Zi-Lan Deng and Jian-Wen Dong*

State Key Laboratory of Optoelectronic Materials and Technologies, Sun Yat-sen University, Guangzhou 510275, China

*dongjwen@mail.sysu.edu.cn

Abstract: We propose a plasmon-induced transparency (PIT) nanocavity for achieving nanoscopic coherent light source. The compact cavity is constructed by a pair of detuned nano-stubs incorporated with four-level gain medium. The PIT response enables the reduction of the coupling loss from cavity to waveguide while keeping the cavity size unchanged, different from the end-facet Fabry-Pérot cavity in which the radiation loss decreases at the cost of size increment. In order to study the lasing behavior of surface plasmon wave in the PIT cavity, the self-consistent finite element method is employed to model the interactions between gain and propagating surface plasmons. The dynamics of the whole lasing process is observed, and the linear output-input relation is obtained for the single mode plasmon lasing. It is demonstrated that smaller stub-pair detuning provides stronger feedback inside the cavity. Consequently, the lasing threshold of pumping rate decreases quadratically with the decreasing of detuning. However, the output-input extraction efficiency will improve when the detuning is not so small. One of the advantages for the proposal is that the lasing output power from the cavity can directly couple towards the metal-dielectric-metal waveguide platform, facilitating the field of integrated plasmonic circuits and molecular-scale coherent light source.

OCIS codes: (240.6680) surface plasmons; (140.3460) Lasers; (250.5300) Photonic integrated circuits; (130.3120) Integrated optics devices.

References and links

1. N. Wang, J. Dong, Y. Yang, Y. Zhang, X. He, C. Wang, B. Li, and G. Yang, "Nanoscopic light sources: General strategy for nanoscopic light source fabrication," Adv. Mater. **23**(26), 2937–2940 (2011).
2. R. F. Oulton, V. J. Sorger, T. Zentgraf, R. M. Ma, C. Gladden, L. Dai, G. Bartal, and X. Zhang, "Plasmon lasers at deep subwavelength scale," Nature **461**(7264), 629–632 (2009).
3. M. T. Hill, M. Marell, E. S. P. Leong, B. Smalbrugge, Y. Zhu, M. Sun, P. J. van Veldhoven, E. J. Geluk, F. Karouta, Y.-S. Oei, R. Nötzel, C.-Z. Ning, and M. K. Smit, "Lasing in metal-insulator-metal sub-wavelength plasmonic waveguides," Opt. Express **17**(13), 11107–11112 (2009).
4. S.-W. Chang, T.-R. Lin, and S. L. Chuang, "Theory of plasmonic Fabry-Perot nanolasers," Opt. Express **18**(14), 15039–15053 (2010).
5. Y.-J. Lu, J. Kim, H.-Y. Chen, C. Wu, N. Dabidian, C. E. Sanders, C.-Y. Wang, M.-Y. Lu, B.-H. Li, X. Qiu, W.-H. Chang, L.-J. Chen, G. Shvets, C.-K. Shih, and S. Gwo, "Plasmonic nanolaser using epitaxially grown silver film," Science **337**(6093), 450–453 (2012).
6. M. Khajavikhan, A. Simic, M. Katz, J. H. Lee, B. Slutsky, A. Mizrahi, V. Lomakin, and Y. Fainman, "Thresholdless nanoscale coaxial lasers," Nature **482**(7384), 204–207 (2012).
7. M. J. H. Marell, B. Smalbrugge, E. J. Geluk, P. J. van Veldhoven, B. Barcones, B. Koopmans, R. Nötzel, M. K. Smit, and M. T. Hill, "Plasmonic distributed feedback lasers at telecommunications wavelengths," Opt. Express **19**(16), 15109–15118 (2011).
8. R.-M. Ma, R. F. Oulton, V. J. Sorger, G. Bartal, and X. Zhang, "Room-temperature sub-diffraction-limited plasmon laser by total internal reflection," Nat. Mater. **10**(2), 110–113 (2011).
9. R.-M. Ma, R. F. Oulton, V. J. Sorger, and X. Zhang, "Plasmon lasers: Coherent light source at molecular scales," Laser Photonics Rev. **7**(1), 1–21 (2013).
10. P. Berini and I. De Leon, "Surface plasmon-polariton amplifiers and lasers," Nat. Photonics **6**(1), 16–24 (2011).
11. S. I. Bozhevolnyi, A. B. Evlyukhin, A. Pors, M. G. Nielsen, M. Willatzen, and O. Albrektsen, "Optical transparency by detuned electrical dipoles," New J. Phys. **13**(2), 023034 (2011).

#191661 - $15.00 USD Received 3 Jun 2013; revised 11 Aug 2013; accepted 16 Aug 2013; published 22 Aug 2013

12. Z. Han and S. I. Bozhevolnyi, "Plasmon-induced transparency with detuned ultracompact Fabry-Perot resonators in integrated plasmonic devices," Opt. Express **19**(4), 3251–3257 (2011).
13. Y. Huang, C. Min, and G. Veronis, "Subwavelength slow-light waveguides based on a plasmonic analogue of electromagnetically induced transparency," Appl. Phys. Lett. **99**(14), 143117 (2011).
14. X. Piao, S. Yu, and N. Park, "Control of fano asymmetry in plasmon induced transparency and its application to plasmonic waveguide modulator," Opt. Express **20**(17), 18994–18999 (2012).
15. G. Wang, H. Lu, and X. Liu, "Dispersionless slow light in MIM waveguide based on a plasmonic analogue of electromagnetically induced transparency," Opt. Express **20**(19), 20902–20907 (2012).
16. N. I. Zheludev, S. L. Prosvirnin, N. Papasimakis, and V. A. Fedotov, "Lasing spaser," Nat. Photonics **2**(6), 351–354 (2008).
17. Z.-G. Dong, H. Liu, J.-X. Cao, T. Li, S.-M. Wang, S.-N. Zhu, and X. Zhang, "Enhanced sensing performance by the plasmonic analog of electromagnetically induced transparency in active metamaterials," Appl. Phys. Lett. **97**(11), 114101 (2010).
18. Z.-L. Deng, J.-W. Dong, H.-Z. Wang, S. H. Cheng, and J. Li, "Power transmission and group delay in gain-assisted plasmon-induced transparency," AIP Adv. **3**(3), 032138 (2013).
19. A. Fang, T. Koschny, and C. M. Soukoulis, "Lasing in metamaterial nanostructures," J. Opt. **12**(2), 024013 (2010).
20. A. Fang, T. Koschny, M. Wegener, and C. M. Soukoulis, "Self-consistent calculation of metamaterials with gain," Phys. Rev. B **79**(24), 241104 (2009).
21. A. Fang, T. Koschny, and C. M. Soukoulis, "Self-consistent calculations of loss-compensated fishnet metamaterials," Phys. Rev. B **82**(12), 121102 (2010).
22. A. Fang, Z. Huang, T. Koschny, and C. M. Soukoulis, "Overcoming the losses of a split ring resonator array with gain," Opt. Express **19**(13), 12688–12699 (2011).
23. Z. Huang, T. Koschny, and C. M. Soukoulis, "Theory of pump-probe experiments of metallic metamaterials coupled to a gain medium," Phys. Rev. Lett. **108**(18), 187402 (2012).
24. S. Wuestner, A. Pusch, K. L. Tsakmakidis, J. M. Hamm, and O. Hess, "Overcoming losses with gain in a negative refractive index metamaterial," Phys. Rev. Lett. **105**(12), 127401 (2010).
25. J. M. Hamm, S. Wuestner, K. L. Tsakmakidis, and O. Hess, "Theory of light amplification in active fishnet metamaterials," Phys. Rev. Lett. **107**(16), 167405 (2011).
26. S. Wuestner, A. Pusch, K. L. Tsakmakidis, J. M. Hamm, and O. Hess, "Gain and plasmon dynamics in active negative-index metamaterials," Philos. Trans. R. Soc. London, Ser. A **369**(1950), 3525–3550 (2011).
27. A. Pusch, S. Wuestner, J. M. Hamm, K. L. Tsakmakidis, and O. Hess, "Coherent amplification and noise in gain-enhanced nanoplasmonic metamaterials: A Maxwell-Bloch langevin approach," ACS Nano **6**(3), 2420–2431 (2012).
28. S. Wuestner, J. M. Hamm, A. Pusch, F. Renn, K. L. Tsakmakidis, and O. Hess, "Control and dynamic competition of bright and dark lasing states in active nanoplasmonic metamaterials," Phys. Rev. B **85**(20), 201406 (2012).
29. C. Fietz and C. M. Soukoulis, "Finite element simulation of microphotonic lasing system," Opt. Express **20**(10), 11548–11560 (2012).
30. A. E. Siegman, *Lasers* (University Science Books, 1986).
31. Y. Matsuzaki, T. Okamoto, M. Haraguchi, M. Fukui, and M. Nakagaki, "Characteristics of gap plasmon waveguide with stub structures," Opt. Express **16**(21), 16314–16325 (2008).

1. Introduction

Miniaturization of photonic devices is a general tendency in nanotechnology. And nanoscopic light source is one of the highlights in integrated nanophotonic devices. Semiconductor nanowire has been shown as a typical small-scale light source [1], but the mode confinement and the device size are constrained by diffraction limit. To further miniature light sources below diffraction limit, plasmon lasers have been demonstrated [2, 3] and attracted wide attentions in the field of nanoscale coherent light sources and amplifiers [4–10]. For most plasmon lasers, a finite segment of plasmon waveguide with the end-facets as a Fabry-Pérot (FP) cavity is used to provide feedback for surface plasmon modes. However, the feedback of end-facet FP cavity is not strong enough due to the low radiation quality factor. Two feasible schemes to mitigate the radiation losses are distributed feedback reflector [7] and total internal reflection cavity [8], which are at the cost of increasing device sizes. It is noted that device size increment may lead to a barrier for the integration between electronic chip and photonic component in optical communication and computing systems. On the other hand, the plasmonic analogue of electromagnetically induced transparency (i.e. PIT) has sharp response due to destructive interferences [11]. A representative PIT structure is metal-dielectric-metal (MDM) waveguide side-coupled to a pair of slightly detuned stub-cavities. In the waveguide-cavity system, the linewidth of the PIT peak can narrow by decreasing the frequency detuning of the two stub cavities, while the total cavity size is kept unchanged [12–15]. Furthermore,

#191661 - $15.00 USD Received 3 Jun 2013; revised 11 Aug 2013; accepted 16 Aug 2013; published 22 Aug 2013

the PIT linewidth can be arbitrarily narrow in the lossless case [13]. It indicates that, the radiation loss (actually the coupling loss from cavity to waveguide) can be well controlled by the frequency detuning of the stub-pair cavity. In principle, it can be reduced to be arbitrarily small without changing the total cavity size.

However, dissipative loss always exists in the plasmonic system. Introducing gain materials into the PIT system is an efficient way to overcome the problem. There are several pioneer works on investigating the interactions between the PIT structure and the gain medium in the frequency domain [16–18]. The gain medium is always described by a simple permittivity with negative imaginary part, and thus the saturation and nonlinearity of gain medium is out of consideration. Therefore, the frequency domain method is quite limited and cannot accurately model the lasing behavior. Fortunately, there is a self-consistent computational scheme solving Maxwell equations along with four level rate equations, which accurately considers the saturation and nonlinearity of the gain medium. This scheme is a time domain method and has been implemented in finite difference time domain (FDTD) method by Soukoulis's group [19–23] and Hess's group [24–28], respectively. Recently, this scheme has also been implemented in finite element method (FEM), which can utilize unstructured grids to accurately model geometries with arbitrary shapes, while only the structured (cubic) grids can be used in FDTD [29]. In addition, the FEM method in Ref [29]. solves separately the pump and probe fields which are represented by slowly varying complex field amplitudes, allowing for large time steps and as a result greatly speeding up the simulation. The self-consistent scheme mentioned above is always employed to study the electromagnetic (EM) behaviors in the periodic gain-assisted metamaterials in terms of radiative plane wave. For modeling propagating surface plasmon wave interacting with four level atomic medium, the FEM method need to be modified but there is still no report so far.

In this paper, we extend the self-consistent method in the FEM framework to model the propagating characteristics of surface plasmons interacting with gain medium. Using the extended self-consistent method, we theoretically investigate the dynamics of the lasing process in the detuned stub-pair cavity which exhibits sharp PIT response. The plasmon laser based on PIT can provide effective feedback for surface plasmon lasing, and at the same time can maintain cavity size in nanoscale. The small size of laser device may benefit the fast and integrated photon-based technologies. Because the PIT response is only one sharp resonance over a broad frequency range, single mode lasing is automatically achieved. In addition, the lasing output power can directly couple to the propagating surface plasmon, unlike the end-facet FP cavity which wastes large part of power into free space. It is promising to realize on-chip subwavelength coherent sources and repeaters in integrated plasmonic circuits.

2. Self-consistent finite element method for surface plasmon lasing

We focus on the PIT structure constructed by a MDM waveguide side-coupled to a pair of slightly detuned stub-cavities. The schematic is shown in Fig. 1(a). The MDM waveguide with the core width of $w = 50nm$ is connected with two stubs with slightly different lengths ($\Delta L = L_1\text{-}L_2$). The frequency detuning of the stub-pair can be tuned by varying ΔL while fixing the total length (e.g. $L_1 + L_2 = 300$nm). The stub corners are filleted with radius of $r = 10nm$ to avoid field singularity and to mitigate the spatial hole burning [30]. In addition, the filleted corners are inevitable in practical experiments [31]. The gain medium is incorporated into the stub-pair cavity (orange region). The dielectric layer is considered as PMMA with the refractive index of $n_D = 1.49$, and the metal is modeled as silver with the Drude model, in the form of $\varepsilon_M(\omega) = \varepsilon_\infty - \omega_p^2 / \omega(\omega + i\gamma)$, where $\varepsilon_\infty = 3.7$, ω_p = 1.38 × 10^{16}Hz, and γ = 2.73 × 10^{13}Hz. The surface plasmon mode is excited by a point source in the middle dielectric layer. Two ports are placed before and after the stub-pair cavity to probe the reflected and transmitted pulse below lasing threshold, as well as the output intensity above threshold. There are also two probe points inside the stub-pair cavity in order to probe the internal cavity intensities and the occupation numbers.

#191661 - $15.00 USD Received 3 Jun 2013; revised 11 Aug 2013; accepted 16 Aug 2013; published 22 Aug 2013

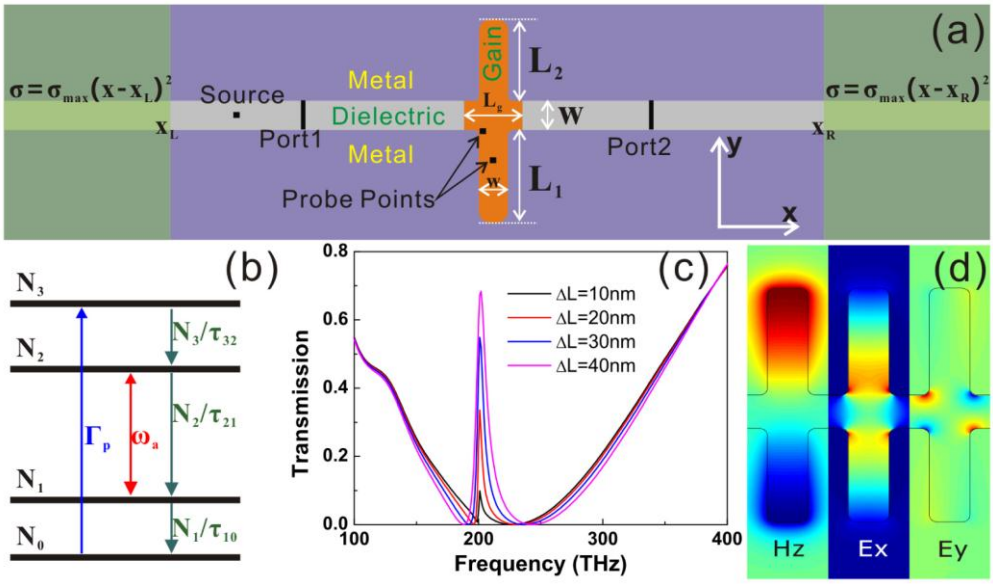

Fig. 1. (a) Schematic of the studied structure. (b) Energy level diagram for the gain medium. (c) Transmission spectra of 'cold cavity' (without gain) for varying detunings. (d) Magnetic and electric field patterns at the PIT frequency for $\Delta L = L_1 - L_2 = 20$nm.

The self-consistent FEM for surface plasmon lasing requires the time domain modeling of the interactions among the EM field, the electric polarization field of the dispersive metal and the gain medium, and the population densities in different energy levels of the gain medium [Fig. 1(b)]. The Drude response of metal is described by the polarization's equation,

$$\frac{\partial^2 \mathbf{P}_D(\mathbf{r},t)}{\partial t^2} + \gamma \frac{\partial \mathbf{P}_D(\mathbf{r},t)}{\partial t} = \varepsilon_0 \omega_p^2 \mathbf{E}(\mathbf{r},t), \tag{1}$$

where $\mathbf{P_D}$ is the polarization density for metal. For the gain medium, it is modeled as four-level quantum system. Consider the electric pumping scheme [Fig. 1(b)], the electrons are pumped from the ground level N_0 to the third level N_3, at a certain pumping rate Γ_p (which is proportional to input power). Then, electrons quickly relax to the metastable level N_2 with relaxation time τ_{32}. Electrons can be transferred from the N_2 to N_1 through spontaneous and stimulated emissions. At last, electrons non-radiatively transfer from N_1 to the ground level N_0 with relaxation time τ_{10}. The lifetime of metastable level is τ_{21}, much larger than τ_{32} and τ_{10}. Consequently, the polarization density $\mathbf{P_a}$ in four-level gain medium obeys the following differential equation:

$$\frac{\partial^2 \mathbf{P}_a(\mathbf{r},t)}{\partial t^2} + \gamma_a \frac{\partial \mathbf{P}_a(\mathbf{r},t)}{\partial t} + \omega_a^2 \mathbf{P}_a(\mathbf{r},t) = -\sigma_a \left(N_2(\mathbf{r},t) - N_1(\mathbf{r},t)\right)\mathbf{E}(\mathbf{r},t), \tag{2}$$

where ω_a is the emission frequency for gain medium, γ_a is the linewidth of the atomic transition and σ_a is a phenomenological isotropic coupling constant. Finally, the occupation number densities at each level obeys the following rate equations,

$$\frac{\partial N_3(\mathbf{r},t)}{\partial t} = \Gamma_p N_0(\mathbf{r},t) - \frac{N_3(\mathbf{r},t)}{\tau_{32}}, \tag{3a}$$

$$\frac{\partial N_2(\mathbf{r},t)}{\partial t} = \frac{N_3(\mathbf{r},t)}{\tau_{32}} + \frac{1}{\hbar \omega_a}\mathbf{E}(\mathbf{r},t) \cdot \frac{\partial \mathbf{P}_a(\mathbf{r},t)}{\partial t} - \frac{N_2(\mathbf{r},t)}{\tau_{21}}, \tag{3b}$$

#191661 - $15.00 USD Received 3 Jun 2013; revised 11 Aug 2013; accepted 16 Aug 2013; published 22 Aug 2013

$$\frac{\partial N_1(\mathbf{r},t)}{\partial t}=\frac{N_2(\mathbf{r},t)}{\tau_{21}}-\frac{1}{\hbar\omega_a}\mathbf{E}(\mathbf{r},t)\cdot\frac{\partial \mathbf{P}_a(\mathbf{r},t)}{\partial t}-\frac{N_1(\mathbf{r},t)}{\tau_{10}}, \tag{3c}$$

$$\frac{\partial N_0(\mathbf{r},t)}{\partial t}=\frac{N_1(\mathbf{r},t)}{\tau_{10}}-\Gamma_p N_0(\mathbf{r},t). \tag{3d}$$

Equations (1)-(3), together with the Maxwell equations for the EM field, can completely describe the dynamics of the lasing system. In the following, we will use the slow-varying amplitude approximation [29] to speed up the calculation. The field can be expanded near the lasing frequency $\omega_1(\approx\omega_a)$,

$$\mathbf{X}(\mathbf{r},t)=\left\lfloor \mathbf{X}_1(\mathbf{r},t)e^{i\omega_1 t}+\mathbf{X}_1^*(\mathbf{r},t)e^{-i\omega_1 t}\right\rfloor/2, \tag{4}$$

where **X** could be any field component, such as **E**, **H**, **D**, **B**, **A**, **P**, **J**, etc. Note that the lasing frequency (ω_1) is between the gain emission frequency (ω_a) and the PIT peak frequency due to the frequency pulling effect [30]. Applying Eq. (4) into Maxwell equations, after some derivation, we can obtain the partial differential equation for the EM field,

$$\frac{1}{\mu_0}\nabla\times\nabla\times\mathbf{A}_1+\varepsilon_\infty\varepsilon_0\left(-\omega_1^2\mathbf{A}_1+2i\omega_1\frac{\partial\mathbf{A}_1}{\partial t}+\frac{\partial^2\mathbf{A}_1}{\partial t^2}\right)+\sigma\left(i\omega_1\mathbf{A}_1+\frac{\partial\mathbf{A}_1}{\partial t}\right)=i\omega_1\mathbf{P}_1+\frac{\partial\mathbf{P}_1}{\partial t}+\mathbf{J}_1, \tag{5}$$

where $\mathbf{A_1}$ is the EM vector potential. From $\mathbf{A_1}$, we can directly obtain the electric field **E** and the magnetic flux density **B** by the following expressions,

$$\begin{aligned}&\mathbf{E}_1(\mathbf{r},t)=-i\omega_1\mathbf{A}_1(\mathbf{r},t)-\partial\mathbf{A}_1(\mathbf{r},t)/\partial t \quad \left(\mathbf{E}(\mathbf{r},t)=-\partial\mathbf{A}(\mathbf{r},t)/\partial t\right),\\ &\mathbf{B}_1(\mathbf{r},t)=\nabla\times\mathbf{A}_1(\mathbf{r},t) \quad \left(\mathbf{B}(\mathbf{r},t)=\nabla\times\mathbf{A}(\mathbf{r},t)\right).\end{aligned} \tag{6}$$

Applying Eq. (4) into Eq. (1), we can obtain the governing equations for the polarization density of the metal, yielding,

$$i\omega_1\mathbf{P}_{D1}+\frac{\partial\mathbf{P}_{D1}}{\partial t}+\gamma\mathbf{P}_{D1}=-\varepsilon_0\omega_p^2\mathbf{A}_1; \tag{7}$$

and applying Eq. (4) into Eq. (2), we can obtain the governing equations for the polarization density of the gain medium, yielding,

$$\frac{\partial^2\mathbf{P}_{a1}}{\partial t^2}+2i\omega_1\frac{\partial\mathbf{P}_{a1}}{\partial t}-\omega_1^2\mathbf{P}_{a1}+\gamma_a\left(i\omega_1\mathbf{P}_{a1}+\frac{\partial\mathbf{P}_{a1}}{\partial t}\right)+\omega_a^2\mathbf{P}_{a1}=\sigma_a(N_2-N_1)\left(i\omega_1\mathbf{A}_1+\frac{\partial\mathbf{A}_1}{\partial t}\right). \tag{8}$$

In addition, Eq. (3) also needs to be rewritten after applying the slow-varying amplitude. Namely, the second term on the right-hand size of Eqs. (3b) and 3(c), representing energy exchange between the EM wave and the electrons, should be replaced by a period averaged value [29],

$$\frac{1}{\hbar\omega_a}\left\langle\mathbf{E}_1\cdot\frac{\partial\mathbf{P}_{a1}}{\partial t}\right\rangle=\frac{1}{2\hbar\omega_a}\left[\left(-i\omega_1\mathbf{A_1}-\frac{\partial\mathbf{A_1}}{\partial t}\right)^*\cdot\left(-i\omega_1\mathbf{P_{a1}}+\frac{\partial\mathbf{P}_{a1}}{\partial t}\right)\right]. \tag{9}$$

In short, Eqs. (5)-(9) are derived from Maxwell equations and polarization equations in the approximation of slow-varying complex amplitude. The advantage of such a set of equations is that the time step is allowed to be even larger than the period of the EM wave. Consequently, the overall time-domain simulation can significantly speed up.

The built-in scattering boundary in the FEM can only efficiently absorb plane waves. To mimic infinite MDM waveguide, an additional absorbing layer is needed to absorb the surface wave in each side. Here, we use a graded conductivity $\sigma = \sigma_{max}(x\text{-}x_{L/R})^2$ in absorbing layers to

#191661 - $15.00 USD Received 3 Jun 2013; revised 11 Aug 2013; accepted 16 Aug 2013; published 22 Aug 2013

gradually absorb the propagating surface plasmon in each side of the MDM waveguide. σ_{max} should be properly chosen to minimize the reflection. To avoid the reflection in the outside boundary, there are additional weak terms on the left and right boundaries,

$$F_{left}\left(\mathbf{A_1}, \mathbf{A}_1\right) = \frac{1}{z_{MDM}} A_{1y}\left(i\omega_1 A_{1y} + \frac{\partial A_{1y}}{\partial t}\right) - \frac{1}{\mu_0} A_{1y} \frac{\partial A_{1x}}{\partial y}, \tag{10}$$

$$F_{right}\left(\mathbf{A_1}, \mathbf{A}_1\right) = \frac{1}{z_{MDM}} A_{1y}\left(i\omega_1 A_{1y} + \frac{\partial A_{1y}}{\partial t}\right) + \frac{1}{\mu_0} A_{1y} \frac{\partial A_{1x}}{\partial y}, \tag{11}$$

where z_{MDM} is the impedance of the MDM waveguide. $\mathbf{A_1}$ (A_{1y}) is the test function of $\mathbf{A_1}$ (A_{1y}). As a whole, Eq. (3), Eq. (5) and Eqs. (7)-(8) are solved by FEM method implemented in COMSOL Multiphysics version 4.3 PDE modules. Equation (5) is implemented in weak form, while Eq. (3) and Eqs. (7)-(8) are implemented in coefficient forms.

3. Lasing dynamics in metal-dielectric-metal waveguide along with stub-pair cavity

3.1 Cold plasmon-induced transparency cavity properties and the comparison with Fabry-Pérot cavity

Figure 1(c) shows the transmission spectra of the 'cold cavity' (no gain) with varying detunings ΔL = 40, 30, 20, 10 nm, respectively. There is a very sharp transmission peak on top of a broad dip background near 200 THz (1500nm), featuring a typical PIT response. If the stub-pair detuning becomes small, the PIT linewidth narrows and the peak transmittance drops down. The magnetic and electric field patterns at the resonant frequency for the ΔL = 20nm case are illustrated in Fig. 1(d), showing strong field enhancements inside the stub-pair cavity. The fields exhibit anti-phase profiles and hot spots in the junction corners. The sharp resonant line-shape and the strong local field enhancement are promising to provide effective feedback. Thus, it may achieve plasmon lasing after considering gain medium. For the PIT cavity without metallic loss, the peak width narrows and the peak value sustains unity when decreasing the frequency detuning ΔL. The radiative Q factor can be obtained from the peak linewidth. Figure 2(a) exhibits that the radiative Q factor increases remarkably with the decreasing of the detuning, and it diverges when the detuning approaches to zero. On the contrary, the radiative Q factor of the end-facet FP cavity is quite different. Here we consider the same MDM waveguide with finite length L as the end-facet FP cavity. We can see from Fig. 2(b) that the radiative Q factor increases almost linearly with the increasing of the cavity length. When the radiative Q reaches 100, the FP cavity length need to be 4μm, while the PIT cavity keeps the total length of 300 nm with the frequency detuning of ΔL = 20nm. It shows that the PIT cavity enables the reduction of the coupling loss from cavity to waveguide while keeping the cavity size unchanged, different from the conventional end-facet FP cavity in which the radiation loss decreases at the cost of size increment.

#191661 - $15.00 USD Received 3 Jun 2013; revised 11 Aug 2013; accepted 16 Aug 2013; published 22 Aug 2013

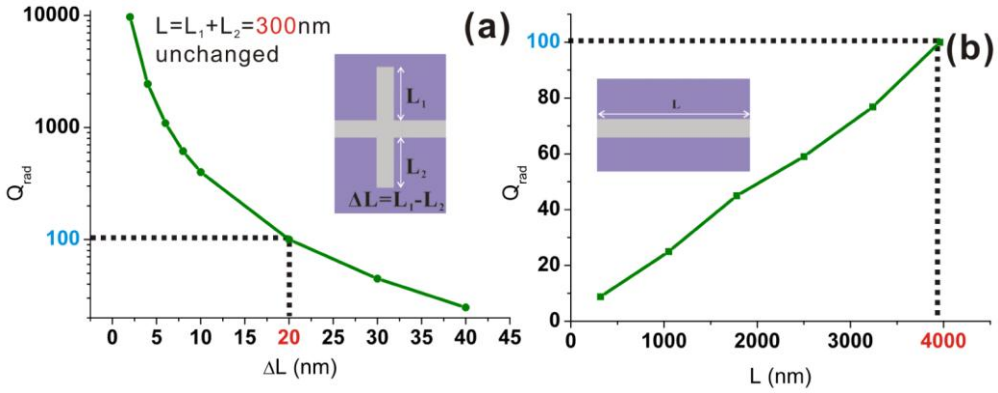

Fig. 2. Radiative quality factor of (a) the PIT cavity and (b) the end-facet FP cavity in the MDM platform for different geometry parameters. For the same radiative quality factor (e.g. 100), the PIT cavity requires $\Delta L = 20$nm with the total length of $L = L_1 + L_2 = 300$nm, while the end-facet FP cavity requires the length to be $L = 4000$nm.

3.2 Surface plasmon propagation below lasing threshold

Next, we will turn to study the surface plasmon propagation after introducing gain medium. The parameters for the gain medium are set as $\tau_{10} = 0.05$ps, $\tau_{21} = 5$ps, $\tau_{32} = 0.05$ps, $\omega_a = 2\pi \times 200$ THz, $\gamma_a = 2\pi \times 10$THz, $\sigma_a = 1e\text{-}4$ C^2/kg, $N_0(t = 0) = 5.0 \times 10^{23} m^{-3}$ [19]. When the occupation number is pumped into a steady population state (after $10\tau_{21} = 50$ps), a weak short probe pulse is launched by setting a point source with the Gaussian form of $J_{srcy} = 10^{-7}\exp(-(t-t_{peak})^2/(2\tau_1^2))$, where $\tau_1 = 0.01$ps (linewidth) and $t_{peak} = 10\tau_{21} + 5\tau_1 = 50.05$ps (peak time).

#191661 - $15.00 USD Received 3 Jun 2013; revised 11 Aug 2013; accepted 16 Aug 2013; published 22 Aug 2013

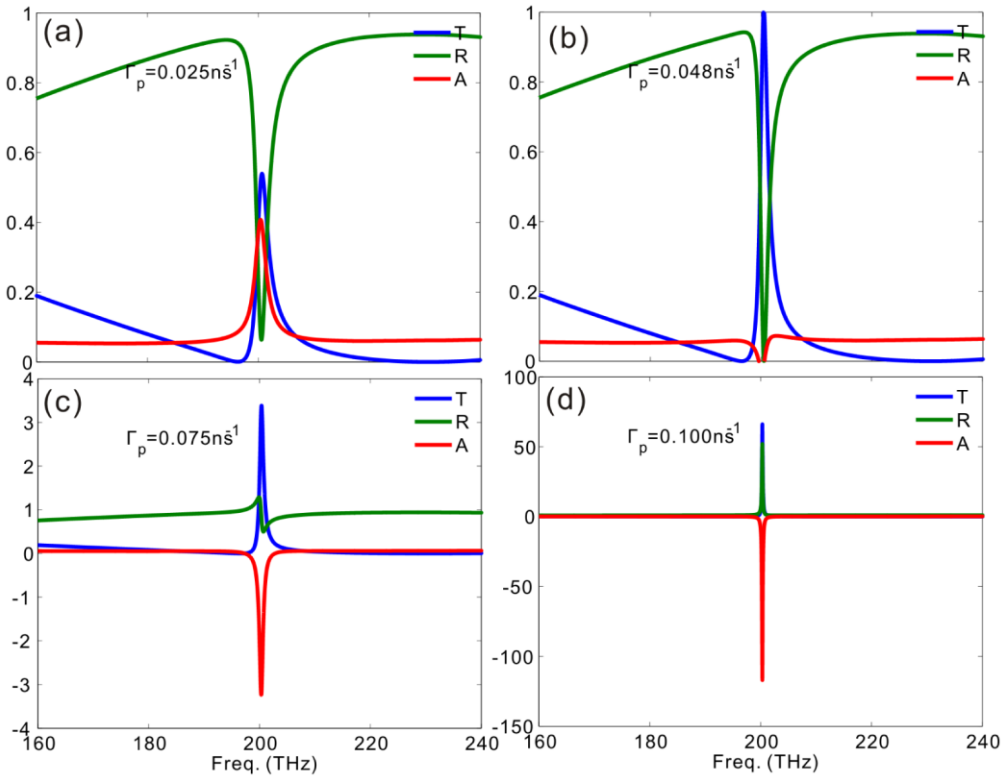

Fig. 3. Evolution of the transmission, reflection and absorption spectra when increasing the pumping rate imposed on the gain medium for $\Delta L = L_1\text{-}L_2 = 20$nm (Media 1).

Below the lasing threshold, the transmission, reflection and absorption (TRA) spectra near 200 THz can be extracted by Fourier transform of the transmitted pulses (port 2) and the reflected pulses (port 1). The representative results are plotted in Fig. 3. One of the prominent properties is that the linewidths of all the spectra become narrower as the pumping rate rises (Media 1). Then we will focus on the variation on the peak (dip) values near 200 THz. For the transmission peak (blue curves in Fig. 3), as the pumping rate increases, it enhances and then reaches unity at $\Gamma_p = 0.048$ ns^{-1} [Fig. 3(b)], indicating that the metallic dissipative loss is fully compensated by the gain medium at $\Gamma_p = 0.048$ ns^{-1}. The transmission peak will exceed unity if we further increase the pumping rate, meaning that surface plasmon wave is amplified when $\Gamma_p > 0.048$ ns^{-1}. For the reflection dip (green curves in Fig. 3), it shows a downward profile and approaches to zero at $\Gamma_p = 0.048$ ns^{-1} [Fig. 3(b)]. It then exhibits the asymmetric Fano line-shape [Fig. 3(c)] and finally becomes an upward peak (Media 1). For the absorption spectra (red curves in Fig. 3), it behaves as anti-absorption picture, showing a dip with negative values in the amplification regime.

Figure 4 reveals a full picture of the PIT peak below lasing threshold. The peak transmittance as a function of the pumping rate is plotted for several detunings of the stub-pair cavity. It is interesting that no matter which the detuning is, the compensation point between dissipative loss and gain is always at $\Gamma_p = 0.048$ ns^{-1} (green dash line at $T_{max} = 1$). This is because the total length of the PIT cavity is fixed at 300 nm. For smaller detuning, the cavity feedback is stronger, and thus the surface plasmon wave can stay longer in the cavity. When the pumping rate is lower than 0.048ns^{-1}, the dissipative loss is superior to the gain. It is in the loss-compensation regime. More surface plasmon wave will be absorbed inside the cavity for smaller detuning. Consequently, the output peak transmittance will become lower (see four curves in $T_{max}<1$ region, from pink to black). On the other hand, longer cavity

#191661 - $15.00 USD Received 3 Jun 2013; revised 11 Aug 2013; accepted 16 Aug 2013; published 22 Aug 2013

lifetime will lead to larger surface plasmon amplification when the pumping rate is larger than $0.048ns^{-1}$, because the dissipative loss is inferior to the gain in the amplification regime ($T_{max}>1$). Therefore, the output peak transmittance will become higher (see four curves in $T_{max}>1$ region, still from pink to black).

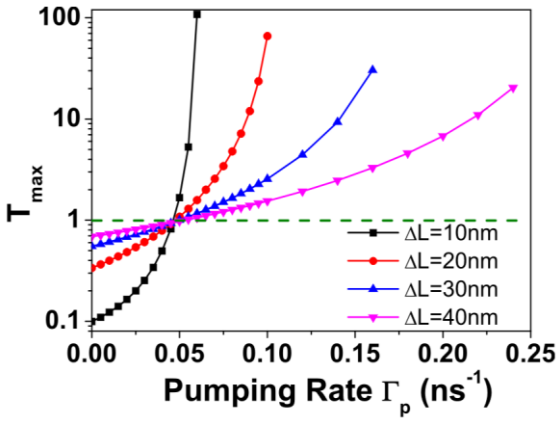

Fig. 4. Peak transmittance as a function of the pumping rate below lasing threshold for different detunings. In the loss-compensation regime ($T_{max}<1$), the smaller the detuning, the lower the peak transmittance. In the amplification regime ($T_{max}>1$), the smaller the detuning, the higher the peak transmittance.

3.3 Plasmon lasing in the plasmon-induced transparency cavity

In the amplification regime, the gain is superior to the dissipative loss (internal cavity loss), but the radiative loss (external cavity loss) could not been overcome if the pumping rate is not high enough. Only if both kinds of losses are surmounted completely, the lasing oscillation will appear. In such situation, the reflected pulse in port 1 and the transmitted pulse in port 2 no longer decay to zero. They first experience relaxation oscillations for a few cycles and then settle into a same steady value [see e.g. Figure 5(a)]. The TRA spectra are meaningless now, since the weak incident pulse is only a perturbation to trigger the lasing to happen. The lasing oscillation is only dependent on the pumping rate. In reality, because of the spontaneous emission, the system will lase without a probe pulse when the pumping rate reaches the threshold. Figure 5(b) shows the dynamics of the population inversion in the lasing process when the pumping rate is above the threshold. The population inversion is pumped to a steady value $2 \times 10^{-3}N_{tot}$ at 50ps, and then the probe pulse enters the cavity. The population inversion declines and the relaxation oscillations occur. The oscillation amplitude is smaller and smaller, and finally approaches a steady value. Note that the steady population inversions in the junction corner are lower than those in the stub center, and are also lower than the average population inversion [Figs. 5(b) and 5(d)]. The reason is that the electric field enhancements in the junction corners are the strongest [Figs. 5(e) and 5(f)]. As a result, more gain is saturated in the junction corners than in other places. The whole dynamic lasing process is shown in the online multimedia (Media 2) (Media 3) (Media 4) (Media 5). From the media, we find that the magnetic field and the electric field oscillate in the same tune. When the population inversion reaches the minimum, the amplitudes of EM fields hit into their maximums. The oscillation strength becomes weaker and weaker and finally towards a steady state.

#191661 - $15.00 USD Received 3 Jun 2013; revised 11 Aug 2013; accepted 16 Aug 2013; published 22 Aug 2013

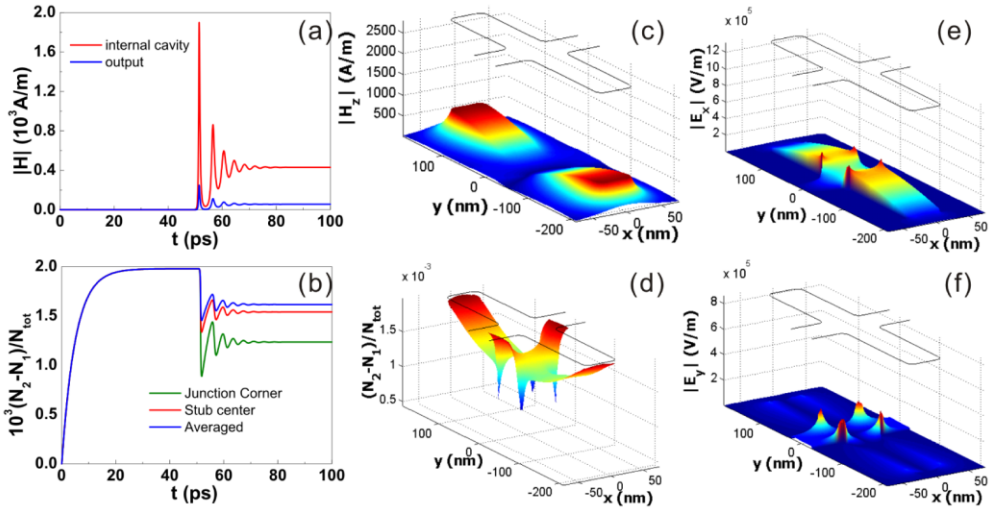

Fig. 5. Dynamics of (a) magnetic field amplitudes and (b) population inversions in the whole lasing process for $\Delta L = 20$nm and $\Gamma_p = 0.2\text{ns}^{-1}$. The spatial profiles of (c) the magnetic field amplitude $|H_z|$ (Media 2), (d) the population inversion $(N_2\text{-}N_1)/N_{tot}$ (Media 3), (e) x-component of electric field $|E_x|$ (Media 4), and (f) y-component of electric field $|E_y|$ (Media 5).

To further investigate the plasmon lasing behavior, we plotted both the output lasing intensity and the internal cavity intensity as a function of the pumping rate for several ΔL in Fig. 6. One can clearly see that, both the output intensity [Fig. 6(a)] and the internal cavity intensity [Fig. 6(b)] increase linearly with the pumping rate after a threshold value. It is the obvious signature of the lasing behavior. By linearly fitting each line in Fig. 6(a) after the amplification-lasing transition point, we can obtain the lasing threshold for each ΔL. Note that the threshold can also be obtained by fitting the line in Fig. 6(b) with similar procedures. The fitted threshold of pumping rate (Γ_p^{th}) as a function of ΔL is shown in Fig. 6(c). It is found that the smaller the detuning, the lower the lasing threshold. The threshold increases quadratically with the detuning, with the fitting formula of $\Gamma_p^{th} = 0.001\Delta L^2 + 0.081$. Although smaller detuning can achieve lower lasing threshold, it leads to lower slope for the curve of output intensity versus pumping rate [inset of Fig. 6(a)], and it also leads to higher slope for the curve of internal cavity intensity versus pumping rate [inset of Fig. 6(b)]. It indicates that the output-input extraction efficiency is lower for smaller detuning case, which is attributed to the fact that the stub-pair cavity with smaller detuning has lower coupling rate to the MDM waveguide. In other words, more power is preserved inside the cavity but less power is coupled to the propagating surface plasmon mode. For example, when the pumping rate is 0.5 ns^{-1}, the radio of the internal cavity intensity over the output intensity is 246, 58, 24 and 12 for ΔL = 10, 20, 30 and 40 nm, respectively. Thus, we will obtain lower lasing threshold but probably lower useful output power for smaller ΔL case. For the extreme case, i.e. $\Delta L = 0$, the lasing threshold is the lowest, but the output intensity will be zero because the lasing power is completely confined inside the cavity. We note that the output intensity slope has a little saturation after ΔL = 30nm [inset in Fig. 6(a)], because large detuning can only provide weak feedback. We also note that, the internal cavity intensities (in order of 10^6) are two orders as large as the output intensity (in order of 10^4) due to the strong field enhancements inside the detuned stub-pair cavity. Furthermore, for a conventional laser, one can tune the reflectivity of the mirror to extract as large as possible power from the laser cavity. Analogously, in the PIT nanolaser, the output power for a given input power can be optimized by tuning ΔL. Figure 6(d) shows the contour for optimum output coupling in the parameter plane of the detuning and the pumping rate. For high pumping rate, large detuning is required to obtain the optimum output intensity, although small detuning has the lower threshold. When the

#191661 - $15.00 USD Received 3 Jun 2013; revised 11 Aug 2013; accepted 16 Aug 2013; published 22 Aug 2013

pumping rate is greater than 1.2 ns^{-1}, ΔL = 30nm is always the optimal detuning, since the slope of the output intensity curve will not increase after ΔL = 30nm.

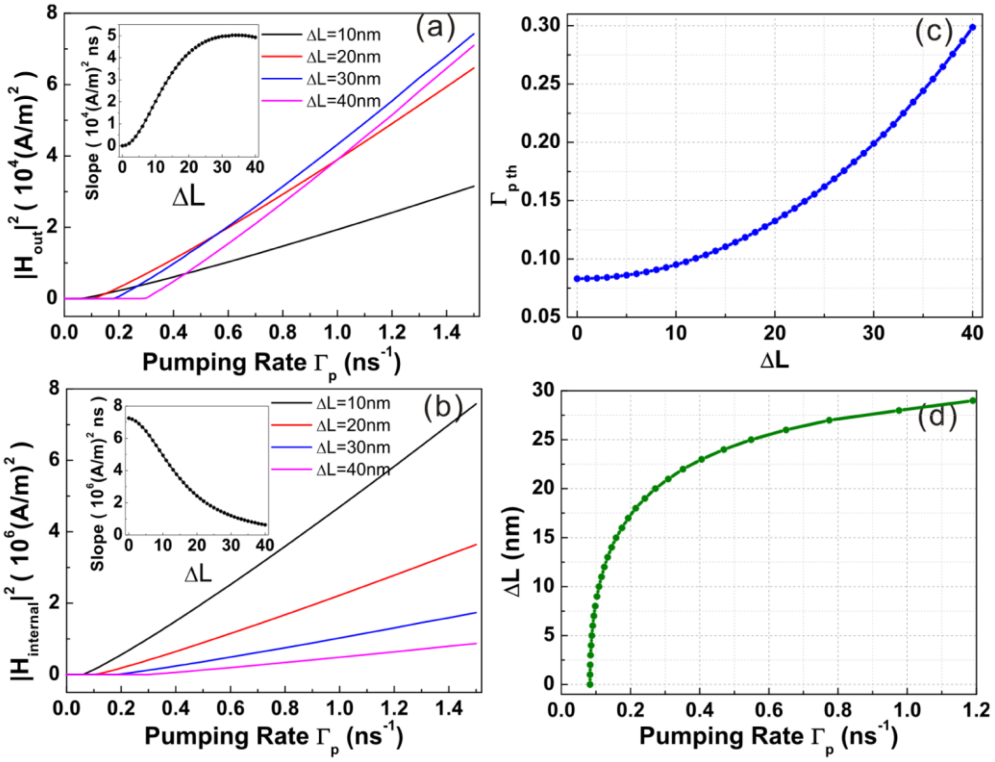

Fig. 6. (a) Output intensity and (b) internal cavity intensity as a function of the pumping rate for differnt detunings ΔL. The insets show the slopes of the lines after lasing threshold. (c) Relationship between the threshold of pumping rate and the detuning ΔL. We can fit the curve as a quadratic function $\Gamma_p^{th} = 0.001\Delta L^2 + 0.081$. (d) The contour for optimal output coupling in the plane of the detuning and the pumping rate.

4. Conclusion

In summary, we studied a new nanolaser scheme based on the PIT response in the detuned stub-pair cavity interconnecting to a MDM waveguide. The PIT cavity can increase the radiative Q factor (and thus the feedback for plasmon lasing) without cavity size increment. The dynamics of the population inversion and the field enhancement in the whole lasing process has been demonstrated by employing an extended version of a self-consistent FEM method. This method can model the interactions between propagating surface plasmons and gain medium in time domain. The transmission behaviors in non-lasing regimes are rich and dependent on the pumping rate. For example, in the loss-compensation region, the smaller the detuning is, the lower the peak transmittance. But it is to the contrary in the amplification region. In the lasing regime, the linear output-input relationship for single mode plasmon lasing is present, and the threshold of the pumping rate decreases quadratically with the decreasing of the detuning. However, the output-input extraction efficiency also decreases with the decreasing of the detuning, since smaller detuning provides stronger feedback. The lasing output power from the PIT cavity can directly couple to propagating surface plasmon mode, promising to realize sources and repeaters in integrated nanophotonic circuits. Although all simulations are performed on a two-dimensional system, the concept is also valid in three-dimension. We have calculated the slot waveguide surrounded by metal in all directions, without gain introduced by frequency domain method. The PIT resonance does

#191661 - $15.00 USD Received 3 Jun 2013; revised 11 Aug 2013; accepted 16 Aug 2013; published 22 Aug 2013

survive except that the resonant peak shifts a little, for the reason of the differences between guided modes in two and three dimension waveguides. Thus, it is reasonable to extend the PIT lasing concept in practical three-dimensional system. But it is hard to fulfill three dimension self-consistent time-domain calculations due to the current limited computer resources. We expect that the PIT laser may be realized in optical experiments, facilitating the field of molecular-scale coherent light source, ultrafast optoelectronic chips, and communications technologies.

Acknowledgments

We gracefully thank Dr. Chris Fietz for his original COMSOL code. This work is supported by the National Natural Science Foundation of China (11274396, 11074311), 973 Program (2014CB931700), the Fundamental Research Funds for the Central Universities (2012300003162498), the Guangdong Natural Science Foundation (S2012010010537). JWD is also supported by the grant for Guangdong Distinguished Young Scientists and the fund for OEMT.